

#### Contents lists available at ScienceDirect

#### Vaccine

journal homepage: www.elsevier.com/locate/vaccine





# A bivalent SARS-CoV-2 subunit vaccine for cats neutralizes both the original ancestral strain and BA.1 Pseudovirus carrying the 453F and 501 T mutation

Ya Zhao <sup>a,b,c</sup>, Zongzheng Zhao <sup>d</sup>, Chuxing Cheng <sup>a,b</sup>, Mingyao Tian <sup>d</sup>, Qiang Zhang <sup>a,b,c,\*</sup>, Meilin Jin <sup>a,b,c,\*</sup>

- <sup>a</sup> College of Veterinary Medicine, Huazhong Agricultural University, Wuhan 430070, China
- <sup>b</sup> National Key Laboratory of Agricultural Microbiology, Huazhong Agricultural University, Wuhan 430070, China
- <sup>c</sup> Hubei Jiangxia Laboratory, Wuhan 430200, China
- d Changchun Veterinary Research Institute, Chinese Academy of Agricultural Sciences, Changchun 132122, China

#### ARTICLE INFO

#### Keywords: bivalent SARS-CoV-2 subunit vaccine cat mutation zoonosis

#### ABSTRACT

The spillover and spillback of severe acute respiratory syndrome coronavirus 2 (SARS-CoV-2) between humans and animals, especially companion animals, threaten global public health security. However, risk assessment of SARS-CoV-2 variants infecting companion animals and the development of corresponding prevention and control technologies are lacking. The aim of this study is to assess the potential risk of enhancement of the infectivity of SARS-CoV-2 in cats owing to mutations at key sites within the spike (S) protein receptor-binding domain (RBD) region and develop an efficient vaccine to cross-neutralize high-risk SARS-CoV-2 variants. The mutations Y453F and N501T synergistically increase the receptor affinity of RBD and cellular infectivity of the pseudovirus and mediate vaccine escape. A novel bivalent subunit vaccine has been developed; it is composed of the S-trimer proteins of the SARS-CoV-2 ancestral strain and the BA.1 strain carrying the 453F and 501 T site mutations. Our data highlight the high degree of risks associated with the Y453F and N501T mutations within RBD in terms of the infectivity and vaccine escape of SARS-CoV-2 in multiple animals. The novel bivalent subunit vaccine can effectively cross-neutralize high-risk SARS-CoV-2 variants in cats, providing reliable technology and theoretical support for curbing the potential transmission of SARS-CoV-2 between humans and animals.

#### 1. Introduction

The coronavirus disease (COVID-19) pandemic, caused by severe acute respiratory syndrome coronavirus 2 (SARS-CoV-2), has had a profound impact on global human health. [1] SARS-CoV-2 is a zoonotic virus with a broad host range that has spread from humans to numerous animal species. [2,3] For example, our earlier study revealed instances where companion animals were infected due to spillover from human patients. [4–6] A growing number of SARS-CoV-2 infections have been reported in lions, tigers, and white-tailed deer. [7,8] Notably, animal-to-human transmission has also occurred. For example, zoonotic transmission from minks to humans was observed in mink farms in the Netherlands in 2020. [9] However, as the main receptor for SARS-CoV-2, angiotensin converting enzyme 2 (ACE2) exists sequence differences between species, leading to marked variation in their susceptibility to

SARS-CoV-2. [10] Therefore, during interspecies transmission, some adaptive mutations usually occur in SARS-CoV-2 to enhance viral susceptibility or antibody escape ability, seriously threatening global public health security.

The spike (S) protein of SARS-CoV-2 is a key envelope glycoprotein that mediates viral host selection and cell entry by specifically recognizing and binding to angiotensin-converting enzyme 2 (ACE2) receptors on host cells. [11,12] The S protein is composed of S1 and S2 subunits, which mainly contain an N-terminal domain (NTD), receptor-binding domain (RBD), and heptad repeat (HR1/2). [13] Among them, the RBD plays a pivotal role in the binding of the S protein with ACE2 and is a promising target for the development of antibody therapeutics and vaccines. [14–17] However, various factors, including replication errors, selective pressure, and cross-species transmission, have driven the virus to continually mutate from its original strain, particularly

<sup>\*</sup> Corresponding authors at: College of Veterinary Medicine, Huazhong Agricultural University, Wuhan 430070, China. E-mail addresses: zhangq\_0401@mail.hzau.edu.cn (Q. Zhang), jinmeilin@mail.hzau.edu.cn (M. Jin).

within the RBD region. The ongoing accumulation of these mutations not only enhances the virus's infectivity and transmissibility but also diminishes the immunogenicity of vaccines and promotes cross-species transmission, thereby posing challenges to pandemic control efforts. [18,19] For example, in mink-related variants, the mutation Y453F in the RBD region enhances the interaction between the S protein and mink ACE2 to facilitate host adaption. [20] In SARS-CoV-2 variants, mutation E484K in the RBD mediates the evasion of antibody neutralization elicited by vaccination or infection. [21] Therefore, assessing the potential risk of enhancement of the infectivity and antibody escape of SARS-CoV-2 in animals because of key mutations within the RBD region and developing efficient vaccines hold critical public health significance.

Although a range of COVID-19 vaccines for humans have been approved and a robust immune barrier has been established within the population, incidents of patients transmitting the virus to animals continue to occur frequently. Companion animals such as cats and dogs often have close contact with humans, and the potential risk of circular transmission of SARS-CoV-2 between humans and companion animals has caused widespread concern. Here, we constructed 28 strains with RBD mutated at the key sites, and we also assessed the potential risk of enhancement of the infectivity of SARS-CoV-2 in companion animals by analyzing the ACE2 affinity of the RBD mutants. [22,23] We further analyzed the effects of high-risk mutations on SARS-CoV-2 antibody escape and developed a novel bivalent subunit vaccine that can efficiently cross-neutralize high-risk SARS-CoV-2 variants in cats. The vaccine will provide an effective control strategy for preventing the potential transmission of SARS-CoV-2 through human-animal-human interactions.

#### 2. Material and methods

#### 2.1. Cells

Vero, Vero E6, and HEK293T cells were purchased from the American Type Culture Collection (ATCC). The cells were cultured in Dulbecco's Modified Eagle Medium (DMEM) supplemented with 10 % fetal bovine serum (FBS) and 100 U/mL penicillin–streptomycin at 37 °C with 5 % CO2. Stable cell lines expressing human ACE2 were constructed and preserved in our laboratory; the cell culture medium was supplemented with 4  $\mu$ g/ml puromycin. HEK293F cells were cultured and preserved in the laboratory. CHO-K1 cells were obtained from Columbia University, commercially licensed, and stored in liquid nitrogen until use. All cells were subjected to regular polymerase chain reaction (PCR) testing, and all results were negative for mycoplasma infection.

#### 2.2. Viruses

The SARS-CoV-2(IVCAS6.7591) and BA.1(IVCAS6.7600) strains used in this study were isolated and preserved at the Wuhan Institute of Virology. All viral experiments were conducted in a Biosafety Level 3 (BSL-3) laboratory approved by the Wuhan Institute of Virology, Chinese Academy of Sciences, as well as Changchun Veterinary Research Institute Biosafety Laboratory, Chinese Academy of Agricultural Sciences, Changchun.

#### 2.3. Ethics approval statement

The animal study fully complied with animal welfare requirements and obtained approval from the Ethics Review Committee of Huazhong Agricultural University and Wuhan Institute of Virology. This study was conducted under their guidance (ID Number: 202208220001 and WIVA17202201). Virus inoculations were performed on animals under anesthesia, using avertin for K18-hACE2 mice and hamsters, and using isoflurane for cats, in efforts to minimize animal discomfort. The sample size for animal experiments was determined based on the standards set by the Animal Ethics Committee.

#### 2.4. Bivalent subunit protein production

To generate the secreted S-trimer fusion proteins of the prototype and BA.1 variant carrying 453F and 501 T mutations, these two segments of the spike protein ectodomain (amino acid residues 16–1209 with a 6P mutation) were separately fused with an N-terminal signal peptide and a C-terminal region containing the T4 foldon, human rhinovirus (HRV) 3C, and Twin-strep-His10. These sequences were codon-optimized and synthesized at Tsingke Biotechnology before being individually inserted into the pCMV-GS expression vector. The plasmids were transfected into CHO-K1 cells. In the presence of 25  $\mu$ M methionine sulfoximine (MSX), stable clones were obtained through limited dilution. The two proteins were separated by affinity chromatography, ion exchange, and gel filtration.

#### 2.5. Production of prototype or mutant RBD proteins

Plasmids expressing the prototype-RBD or mutant-RBD, whose C-terminal was fused with the human immunoglobulin G1 (IgG1) Fc, were constructed and transfected into HEK293F cells for expression without the need for purification. Only the secreted protein was collected for subsequent experiments. One day before starting the transfection experiment, cells should be seeded at a density of  $1\times10^6$  cells per milliliter. In the plasmid transfection process, the plasmid was used at a concentration of 1  $\mu g$  per milliliter of cell suspension. Simultaneously, polyethylenimine (PEI) at a concentration of 1 mg/mL is added in a 3:1 ratio to the plasmid. The cells were then cultured at 37 °C, 5 % CO2, and 120 rpm. At 24 and 96 h post-culture, 3.5 % of the supplementary culture medium was added. After four days of cultivation, the cell supernatant was collected, centrifuged, and filtered; a part of the samples was subjected to western blotting to assess the protein expression levels, whereas the remaining samples were stored at  $-80\,^{\circ}\text{C}$  for future use.

#### 2.6. Screening for binding sites of RBD affecting receptor affinity in cats

The BLI experiment was conducted on a FortéBio Octet RED96 instrument using a protein A biosensor to analyze the kinetics of binding of prototype- or mutant-RBD to cat ACE2 proteins (*Felis catus*, NCBI Accession: XP\_023104564.1). prototype- or mutant-RBD proteins from the cell culture supernatant were immobilized onto the biosensor to achieve a 4-nm capture response. After stabilizing with 0.02 % PBST (phosphate-buffered saline [PBS] with 0.02 % Tween 20) for 120 s, the biosensor was exposed to a two-fold serial dilution of canine, feline, and mink ACE2 receptor proteins for 180 s. Subsequently, the biosensor was dissociated in the presence of 0.02 % PBST for 180 s. Values were adjusted by subtracting values obtained for the buffer control group to account for nonspecific binding. Association rate constant (Kon), dissociation rate constant (Koff), and equilibrium dissociation constant (KD) were calculated using FortéBio data analysis software (Octet Analysis Studio version 12.2), employing a 1:1 binding and global fitting model.

### 2.7. Flow cytometry screening for binding sites of RBD affecting receptor affinity in cats

HEK293T cells with a fusion rate of 80–90 % were transfected to express enhanced green fluorescent protein (EGFP)-tagged ACE2 receptors from cats. Transfected cells were incubated with prototype- or mutated-RBD proteins of SARS-CoV-2C-terminally fused with human IgG1 Fc and stained with anti-human IgG1 Fc-647 for flow cytometric analysis. Values are presented as the percentage of RBD-Fc-positive cells among the ACE2-expressing cells (EGFP-positive cells). All experiments were independently conducted three times.

#### 2.8. Pseudovirus neutralization assay

Neutralization of SARS-CoV-2 was assessed by performing a single round of infection assay with a lentivirus-based pseudovirus. Full-length expression plasmids for the S genes of SARS-CoV-2 prototype and Omicron BA.1 were codon-optimized, synthesized, and cloned into the pCMV vector (Sino Biological). Single point mutations, including K417T, Y453F, Q493K, Q498H, N501T, and Y453F, as well as a double point mutation, Y453F and N501T, were introduced into the S genes of SARS-CoV-2 prototype via site-directed mutagenesis. The titer of the pseudoviruses was determined by calculating the viral copy numbers based on the results of real-time quantitative PCR targeting the LTR sequence. Pseudoviruses were generated by co-transfecting HEK293T cells with an envelope (Env)-deficient human immunodeficiency virus (HIV) backbone (pNL4-3.Luc.RE) and a vector expressing the S protein. Pseudoviruses were mixed in duplicates with sera at an initial 30-fold dilution and six consecutive three-fold dilutions. The mixtures were then added to monolayers of 293 T-hACE2 cells in duplicates. After 48 h of infection, the cells were lysed, and firefly luciferase activity was detected using a luciferase assay system (Promega) on a microplate reader (Tecan Spark 10 M). The IC50 values of the sample were calculated using GraphPad Prism software version 8.0.2. The reported values represent the geometric means of two independent assays.

#### 2.9. Enzyme-linked immunosorbent assay (ELISA)

Assays were performed in 96-well microtiter plates (Thermo Fisher Scientific) coated with 100 µL (1 µg/mL) of recombinant SARS-CoV-2 prototype and BA.1 spike RBD proteins. The plates were incubated at 4°C overnight, blocked for 2h at 37°C using 5 % bovine serum albumin (BSA), and washed five times with PBST (PBS with 0.05 % Tween 20). Serum samples were initially diluted by a factor of 100 and subsequently subjected to eight consecutive ten-fold dilutions. Next, the samples were serially diluted in 5 % BSA in PBST, added to plates, incubated for 1 h at 37°C, and then washed five times with PBST. Goat anti-mouse and hamster IgG-HRP (SouthernBiotech) or rabbit anti-cat and dog IgG-HRP (Biodragon) was diluted in 5 % BSA before adding to the wells, and the solutions were incubated for 1 h at 37 °C. The plates were washed five times with PBST before adding the tetramethylbenzidine (TMB) substrate. The reactions were stopped using the TMB stop solution. Optical density (OD) measurements were recorded at 630 nm; titers were calculated by four-parameter logistic curve fitting using GraphPad Prism software (version 8.0.2).

# 2.10. Animal immunization and SARS-CoV-2 challenge experiments using adjuvants

CpG 1018 is purchased by PAPP Bio. CpG 1018, a TLR-9 agonist, is a synthetic CpG-B oligonucleotide with a phosphorothioate-modified backbone and sequence 5′-TGACTGTGAACGTTCGAGATGA-3′. GEL02 was produced by SEPPIC according to GMP. Before each immunization, the bivalent S-trimer subunit vaccine was thoroughly mixed with the adjuvant at a 7:1 ( $\nu/\nu$ ) ratio by gentle inversion in a 1 mL total immunization preparation containing 1 mg CpG 1018.

#### 2.11. K18-hACE2 transgenic mice infection experiment

Initially, the mice were anesthetized using isoflurane gas, followed by administration of deeper anesthesia through intraperitoneal injection of avertin. Infection was carried out by intranasally administering 30  $\mu L$  of the sample containing 10,000 TCID50 of the original strain or the BA.1 strain of SARS-CoV-2 to 4–6-week-old K18-hACE2 mice. After infection, weight and survival rates were monitored daily for 5–7 days, and subsequently the remaining animals were euthanized. Lung tissues were dissected and placed into 2 mL tubes containing magnetic beads for subsequent viral load testing through homogenization. Additionally, a

segment of the lung tissue was fixed in a tissue fixative to prepare pathological tissue sections and immunohistochemistry slides.

#### 2.12. Cat and dog immunization

Dogs and cats were immunized with a bivalent subunit vaccine, prepared by mixing 50  $\mu g$  of the sample (containing 25  $\mu g$  SARS-CoV-2 prototype S-trimer and 25  $\mu g$  BA.1 with 453F and 501 T) with CpG1018/Gel02, subcutaneously over the neck, three weeks apart. Blood was collected weekly after the first immunization until two weeks after the second immunization, and then every two weeks thereafter. Levels of anti-spike RBD and neutralizing antibodies were measured by ELISA and lentivirus-based pseudoviral neutralization tests. Routine serum biochemical parameters in dogs and cats were measured, including liver function markers (ALP, ALT, TBIL, GLOB), renal function indicators (BUN, CRE, PHOS), pancreatic enzymes (AMY), and metabolic parameters (GLU, TP, ALB, Ca, Na $^+$ , K $^+$ ).

#### 2.13. Cat infection experiments

After subcutaneous immunization with two doses of the bivalent vaccine, the cats were infected intranasally using  $1\times 10^6$  TCID50 of the SARS-CoV-2 prototype strain and observed continuously for five days. The animals were euthanized at two time points on the third and fifth days, and samples including nasal turbinates, trachea, lung tissue, and pancreas were collected, fixed with 4 % paraformaldehyde, and subjected to HE staining for pathological analysis.

#### 2.14. Viral RNA extraction and measurement

Viral RNA in the tissue homogenate was extracted using the QIAamp Viral RNA Mini Kit (Qiagen, Germany) following the manufacturer's instructions. Quantification of viral RNA in each sample was performed by reverse transcription quantitative polymerase chain reaction (RT-qPCR) using an assay kit (Sansure Biotech Corporation). The CT values were converted to viral copy numbers based on a standard curve established in our laboratory.

#### 2.15. Histopathology and immunohistochemistry

Lung tissues were fixed with 4 % paraformaldehyde, followed by paraffin embedding. Each paraffin-embedded tissue sample was cut into 5-µm-thick sections. After dewaxing and rehydration, the tissue sections were stained with hematoxylin-eosin (HE) for histopathological analysis. The sections were evaluated using an AxioVert 200 M optical microscope (Zeiss, Oberkochen, Germany). Stained slides were scanned with a Pannoramic slide scanner (Pannoramic 250/MIDI), and the morphological changes were assessed by a semi-quantitative score. For the scoring, a dual histopathology scoring system adapted from was used to assess pathological severity [24]. For each criterion, a score 0 = absent,  $1=1\text{-}10\,\%$  of lung section,  $2=11\text{-}25\,\%$  of lung section,  $3=26\text{-}50\,\%$  of lung section, and  $4\geq50\,\%$  of lung section affected.

#### 2.16. Structural visualization and analysis

This study utilized existing protein structures from the Protein Data Bank (PDB), including human ACE2 (PDB ID: 1R42), cat ACE2 (PDB ID: 7C8D), and dog ACE2 (PDB ID: 7E3J). Additionally, mink ACE2 structure was predicted using AlphaFold2. Molecular docking simulations and protein structure visualizations were performed in Discovery Studio (v19). Further visualization and image generation were also carried out using PyMOL (Version 2.5.2).

#### 2.17. Statistical analysis

Statistical analyses were carried out using GraphPad Prism software

(GraphPad8.0.2), employing non-paired Student's t-tests or one-way analysis of variance (ANOVA) when suitable. Bidirectional ANOVA was applied as needed. A p value <0.05 was deemed statistically significant. \*p < 0.05 signifies a significant difference, \*\*p < 0.01 denotes a high level of significance, and \*\*\*p < 0.001 highlights an exceptionally significant difference.

#### 3. Results

### 3.1. Screening of RBD mutation sites enhancing ACE2 affinity and antibody escape in cats

To explore the impact of SARS-CoV-2 mutations on ACE2 receptor affinity in susceptible cats, we generated the ancestral RBD and 28 mutated RBDs. These mutations encompassed key variants of concern (VOCs) and previously reported mutations such as Q498H, Q493K, and Y453F, which have been linked to cross-species transmission in mice and minks. We employed the highly sensitive biolayer interferometry (BLI) technique to accurately measure the in vitro receptor binding affinity of these mutants. Using a protein A biosensor, we captured RBD mutant proteins tagged with human immunoglobulin G1 (IgG1) Fc; this method streamlined the process by bypassing protein purification and significantly enhanced throughput (Fig. 1a).

As demonstrated in Fig. 1b, the affinities of RBD mutants K417T, Y453F, Q493K, Q498H, and N501T for cat ACE2 were 2.55–8.55-fold higher than that of the original RBD (Fig. 1b), implying that these mutated sites enhanced the invasion capability of SARS-CoV-2 into cats. Next, to investigate the effects of these mutations on antibody escape, we generated a lentivirus-based pseudovirus containing the above five mutations and performed a neutralizing assay using cat immune serum from the SARS-CoV-2 prototype strain-inactivated vaccine. As shown in Fig. 1c, the Y453F and N501T mutations significantly reduced antibody neutralization in cats; however, the K417T, Q493K and Q498H mutations had no significant impact. In vitro binding assays demonstrate that the Y453F and N501T mutations may enhance the cross-species

transmission potential of the virus between humans and felines.

## 3.2. Y453F and N501T mutations synergistically enhance infectivity and vaccine escape of SARS-CoV-2 in cats

To assess whether Y453F and N501T mutations synergistically enhance infectivity and vaccine escape of SARS-CoV-2, we generated RBD mutants and pseudoviruses, both of which contained the doublesite mutations Y453F and N501T. First, we compared the receptor affinities of the RBD single-site and double-site mutants using BLI. As shown in Fig. 2a, compared with the single-point mutations Y453F and N501T, the double-point mutation Y453F-N501T further enhanced the affinity of RBD for feline ACE2 and did not affect or even enhanced its affinity for human ACE2. This indicates that the Y453F and N501T mutations can synergistically enhance the affinity for binding to the feline receptor ACE2 (Supplementary Fig. S1). To verify this, we designed a dual-color flow cytometric assay based on feline ACE2expressing live cells overexpressing EGFP green fluorescent tags (Fig. 2b). The cat ACE2 receptor fused with EGFP was efficiently expressed in 293 T cells and localized on the cell membrane (Fig. 2c). The dual-color flow cytometric assay results showed that the rate of binding of the prototype RBD protein to the cat ACE2 was 81.1 %; the binding rates of RBD Y453F, RBD N501T, and RBD Y453F-N501T to cat ACE2 were 87.8 %, 88.8 %, and 90.8 %, respectively (Fig. 2d). This result verified that both Y453F and N501T mutations enhance the binding capacity of viral proteins to feline ACE2 at the cellular level, with the double mutant exhibiting synergistic effects.

In addition, we compared the invasion capabilities of the original strain, single-site mutants, and double-site mutant pseudoviruses in a 293 T cell line stably expressing feline ACE2. As shown in Fig. 2e, the Y453F-N501T double-point mutated pseudovirus demonstrated a significantly enhanced ability to invade feline receptor ACE2 cells compared to that shown by the RBD, Y453F, and N501T pseudoviruses.

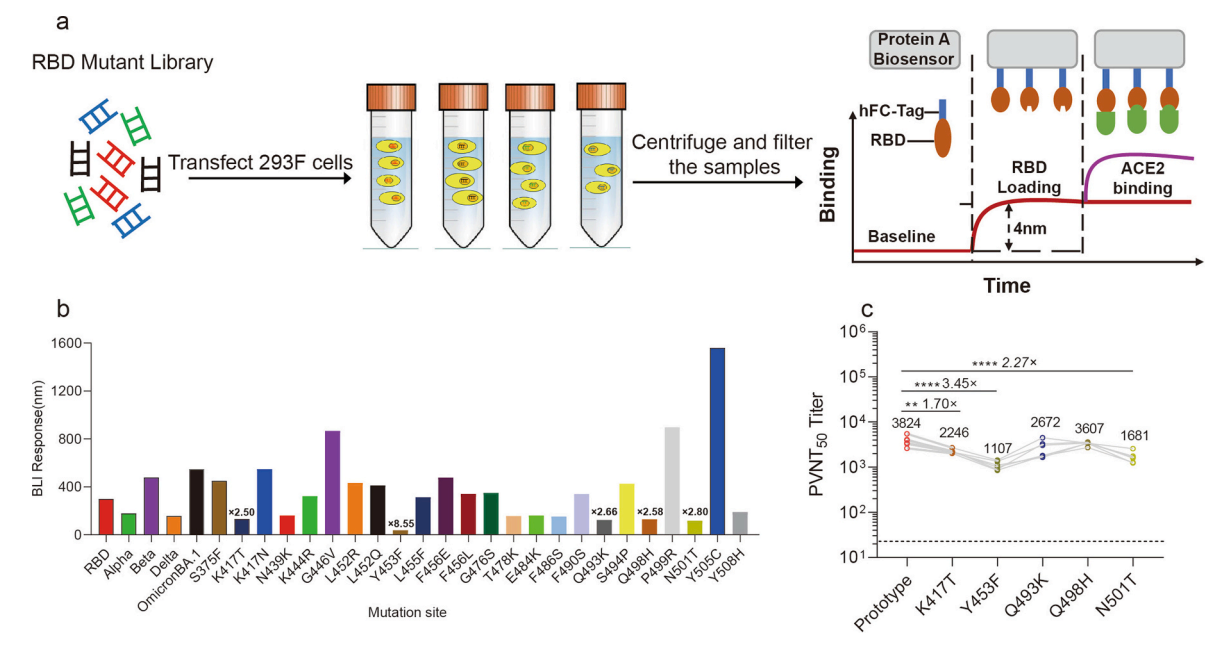


Fig. 1. Screening of receptor-binding domain (RBD) mutation sites enhancing angiotensin-converting enzyme 2 (ACE2) affinity and antibody escape in cats. (a) Schematic diagram for screening RBD mutants that affect the affinity of feline ACE2. The Protein A biosensor (SARTORIUS) was employed to capture RBD mutant proteins expressed and secreted by 293F suspension cells. The C-terminus of these proteins was fused with human IgG1 Fc, with a consistent protein loading of 4 nm on the biosensor. Recombinant feline ACE2-his protein, serially diluted two-fold, was used as the analyte. (b) Assessment of the affinity between various mutant strains and feline ACE2. The fold change in affinity was calculated by dividing the affinity of the mutant strains by that of the wild-type RBD when interacting with feline ACE2. (c) Evaluation of the neutralizing activity of pseudoviruses carrying single-point mutations (K417T, Y453F, Q493K, Q498H, and N501T) against the serum from cats immunized with two doses of inactivated SARS-CoV-2 prototype vaccine, conducted through a pseudovirus neutralization assay.

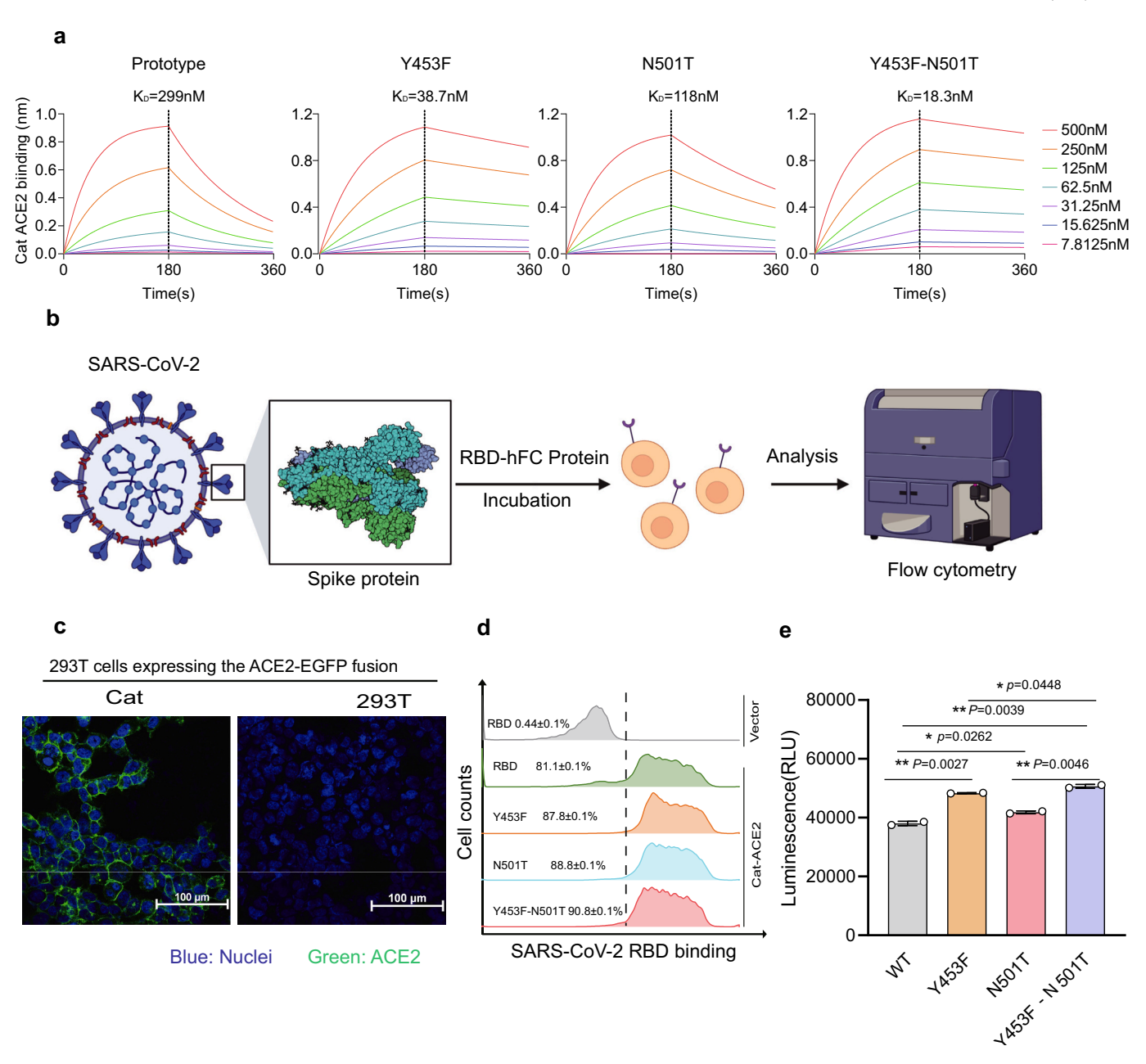


Fig. 2. Y453F and N501T mutations synergistically enhance the infectivity and vaccine escape of severe acute respiratory syndrome coronavirus 2 (SARS-CoV-2) in cats. (a) The binding affinity of cat ACE2 for purified Fc-tagged RBD, Y453F-RBD, N501T-RBD, and double-mutant Y453F-N501T RBD proteins was measured using biolayer interferometry (BLI). (b) Schematic diagram showing the efficiency of binding of cat ACE2 with the viral spike protein and its role in mediating viral entry. (c) C-terminally EGFP-tagged feline ACE2 was successfully expressed in 293 T cells. (d) Cat ACE2-EGFP-expressing cells were dissociated into single cells by trypsinization and incubated with recombinant RBD proteins, including Fc-tagged RBD, Y453F, N501T, and Y453F-N501T mutants. The cells were subsequently stained with Alexa Fluor 647-conjugated goat anti-human immunoglobulin G (IgG) Fc (Southern Biotech) and analyzed using flow cytometry. Binding efficiency is expressed as the percentage of RBD-Fc red-positive cells among green ACE2-expressing cells. This experiment was independently replicated thrice. (e) SARS-CoV-2, Y453F, N501T, and Y453F-N501T pseudovirus infection assays were conducted using 293 T cells expressing cat ACE2. Infectivity was quantified by measuring luciferase activity in the cells. The titer (copy number) and infection efficiency of the pseudovirus meet the experimental requirements (Supplementary Fig. S2). (For interpretation of the references to color in this figure legend, the reader is referred to the web version of this article.)

## 3.3. Y453F and N501T mutations may pose a potential high risk for interspecies transmission of SARS-CoV-2 to multiple animals

To elucidate the impact of the Y453F and N501T mutations on the interaction of mutated proteins with feline ACE2, we performed molecular docking to compare the structures of CatACE2-RBD and CatACE2-RBD with the Y453F and N501T mutations (Fig. 3a). Residues near position 501 in the RBD and their corresponding binding residues in CatACE2 were analyzed. Specifically, CatACE2-Y41 formed polar hydrogen bonds with the RBD residues T500 and N501. The N501T

mutation brought CatACE2-Y41 closer to RBD-T500 and RBD-T501, thereby shortening the hydrogen-bond distances. As a result, the N501T mutation enhanced the binding affinity of the RBD to CatACE2 (Fig. 3b).

Regarding the Y453F mutation, the phenyl ring of RBD-F453 formed non-covalent  $\pi$ - $\pi$  stacking interactions with the imidazole ring of CatACE2-H34 (Fig. 3c). This interaction increased the binding affinity of RBD-Y453F to CatACE2. Next, we analyzed the amino acid sequence conservation at positions 34 and 41 in ACE2 proteins from different species, including humans, cats, dogs, minks, cattle, sheep, goats,

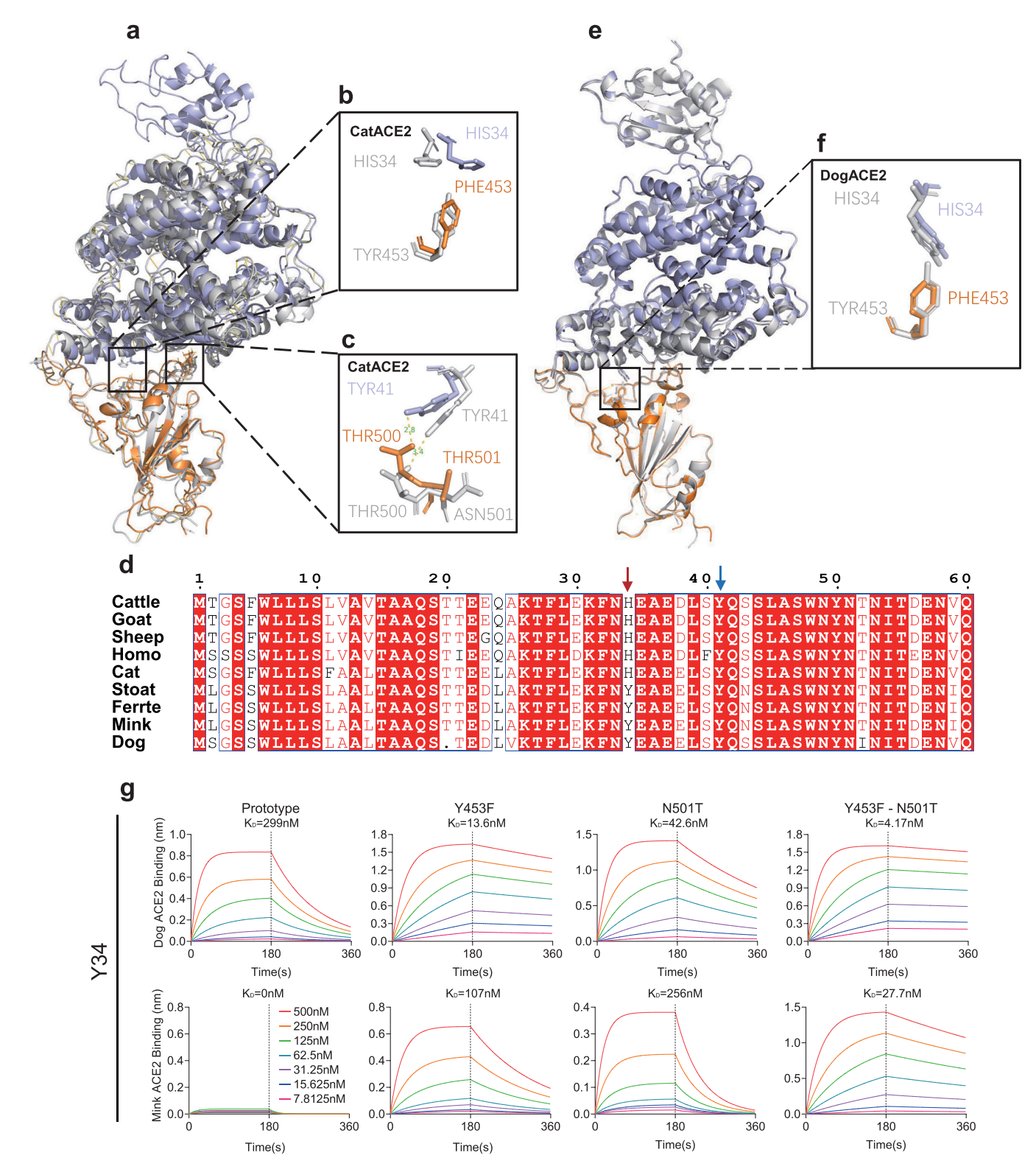
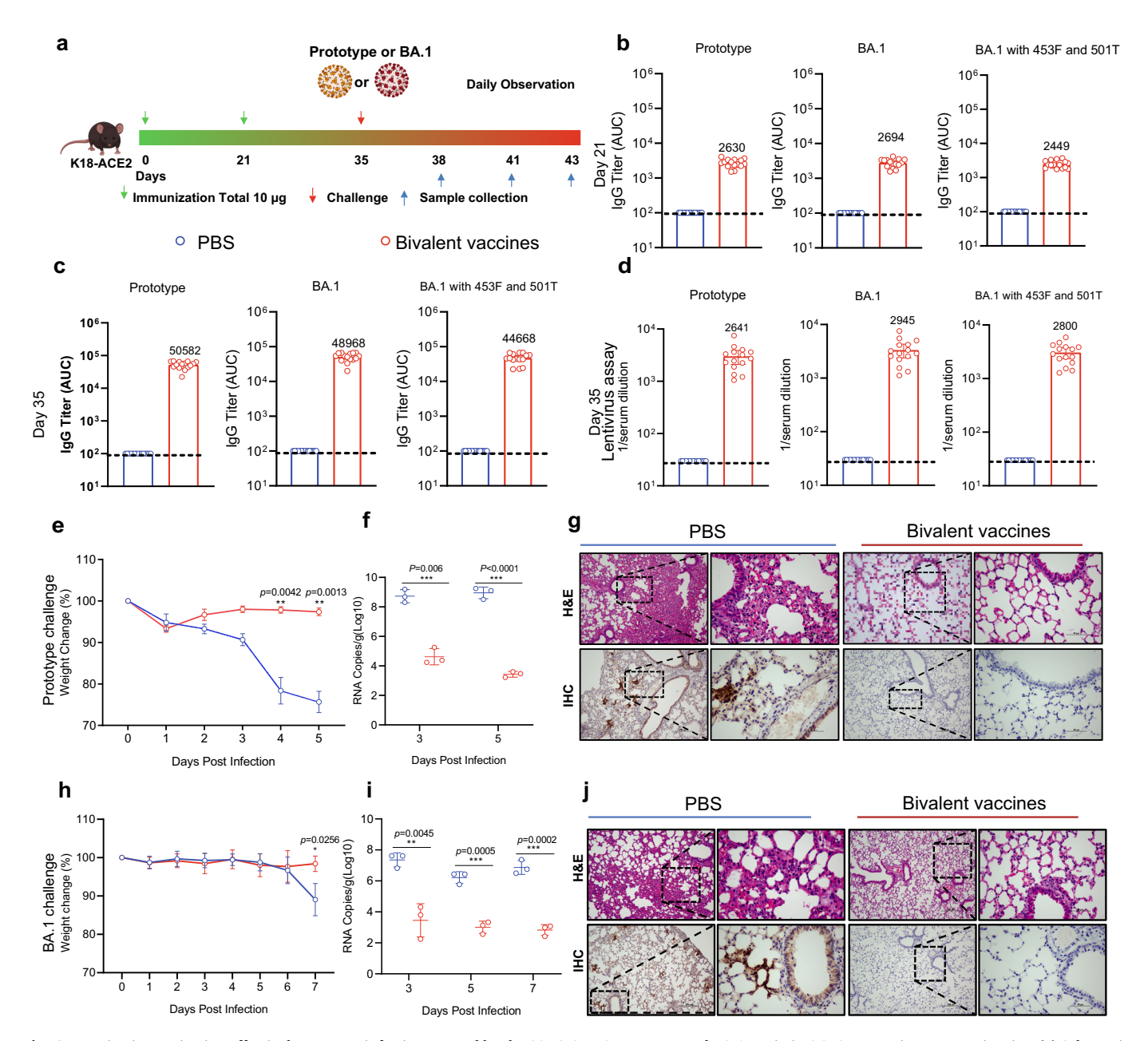


Fig. 3. Y453F and N501T mutations result in a potentially high risk of interspecies transmission of SARS-CoV-2 among multiple animals. (a) Structural analysis of the interaction between the SARS-CoV-2 spike protein and feline ACE2 receptor (PDB ID: 7C8D) was conducted using crystal structures obtained from the Protein Data Bank (PDB). The structures of CatACE2-RBD and CatACE2-RBD with the Y453F and N501T mutations are overlaid for comparison. CatACE2 and RBD Y453F-N501T are indicated in purple and orange, respectively. (b) CatACE2 Y41 and RBD N/T501 are overlaid on both structures. (c) CatACE2 H34 and RBD Y/F453 are overlaid on both structures. CatACE2 H34 and RBD Y/F453 are depicted as sticks and labeled. (d) Critical changes in the virus-contacting hotspot residues 34 (red arrow) and 41(blue arrow) in ACE2 from different host species. Sequence logos were generated using ESPript (https://espript.ibcp.fr/ESPript/cgi-bin/ESPript.cgi/). GenBank accession numbers for ACE2 are as follows (Table S1) (e) The structures of DogACE2-RBD and DogACE2-RBD with Y453F and N501T mutations are overlaid for comparison. DogACE2 and RBD Y/F453 are indicated in purple and orange, respectively. (f) DogACE2-Y34 and RBD Y/F453 are overlaid in both structures. DogACE2-Y34 and RBD Y/F453 are depicted as sticks and labeled. (h) Binding affinities of dog and mink ACE2 (Y34) with purified Fc-tagged RBD, Y453F-RBD, N501T-RBD, and double-mutant RBD Y453F-N501T proteins were measured using a BLI assay. (For interpretation of the references to color in this figure legend, the reader is referred to the web version of this article.)

ferrets, and stoats. As shown in Fig. 3d, tyrosine at position 41 was highly conserved, whereas the conservation of position 34 among the nine ACE2 types was relatively low, with histidine (humans, cats, cattle, sheep, and goats) and tyrosine (dogs, minks, ferrets, and stoats) being predominant. These results indicate that the N501T mutation in RBD

may potentially enhance binding affinity to ACE2 across multiple animal species, though further validation across broader taxonomic groups is warranted. To assess whether the RBD Y453F mutation has a similar potential wide-spectrum effect, we used molecular docking to compare the structures of DogACE2-RBD and DogACE2-RBD Y453F mutant



**Fig. 4.** Vaccine immunization effectively prevents infections caused by the SARS-CoV-2 prototype and BA.1 strain in ACE2-expressing transgenic mice. (a) Schematic representation of the immunization, blood collection, challenge, and sample collection processes in mice. (b) Serum antibody binding to SARS-CoV-2 prototype, BA.1, and Y453F-N501T double-mutant RBD proteins as measured by enzyme-linked immunosorbent assay (ELISA) on day 21. (c) Serum antibody binding to SARS-CoV-2 prototype, BA.1, and Y453F-N501T double-mutant RBD proteins as measured by ELISA on day 35 (n = 15 mice per group; geometric mean titers (GMTs) are indicated at the top of the boxes, and LOD is marked by dotted lines). (d) Neutralizing activity of serum on day 35 against pseudoviruses expressing the spike proteins of SARS-CoV-2 prototype, BA.1, and Y453F-N501T double-mutants (n = 15 mice per group, one experiment; GMTs are indicated at the top of the boxes, and LOD is marked by dotted lines). (e) Weight changes were observed over five days post-challenge with TCID50 value of  $10^4$  for the SARS-CoV-2 prototype strain (n = 15 mice per group). (f) Viral RNA loads in lung tissues at 3 and 5 dpi. (g) Hematoxylin-eosin and indirect immunofluorescence staining of lung sections collected at 3 dpi from mice exposed to the SARS-CoV-2 prototype strain and immunized with either control phosphate-buffered saline (PBS) or the bivalent vaccine. Representative images at moderate (middle; scale bars, 200 μm) and high magnifications (bottom; scale bars, 50 μm) are shown. (h) Weight changes were observed over seven days post-challenge with TCID50 value of  $10^4$  for the BA.1 strain (n = 15 mice per group). (i) Viral RNA levels in lung tissues at 3, 5, and 7 dpi. (j) Hematoxylin-eosin and indirect immunofluorescence staining of lung sections collected at 3 dpi from mice exposed to the BA.1 strain and immunized with either control PBS or the bivalent vaccine. Representative images at moderate (middle; scale bars, 200 μm) and high magnifications (bott

(Fig. 3e). Regarding the Y453F mutation, the phenyl ring of RBD F453 formed stronger hydrophobic interactions with the phenyl ring of DogACE2-Y34 compared to the weaker interactions shown by the hydrophilic side chain of RBD Y453. Molecular docking simulations suggested that the Y453F mutation could potentially improve RBD-DogACE2 binding interactions, with tyrosine at position 34 appearing to contribute to the interface stabilization (Fig. 3f). This suggests that the Y453F mutation in the RBD potentially enhances its binding affinity to ACE2 in multiple animal species.

To verify the above hypothesis, we performed BLI to evaluate the impact of RBD F453 and T501 single-point and double-point mutations on the affinities of proteins from two species, dogs and minks, whose ACE2 proteins have a tyrosine residue at position 34. The results revealed that all mutants enhanced the affinities of RBD with dog and mink ACE2 proteins; in particular, the enhancement caused by double-point mutations was most significant (Fig. 3g). In addition, the results of dual-color flow cytometry and pseudovirus entry also demonstrated that RBD Y453F and N501T mutations significantly enhanced the binding and entry capabilities of the virus to receptors in dogs and minks.

## 3.4. SARS-CoV-2 bivalent subunit vaccine protects hACE2-expressing transgenic mice against SARS-CoV-2 prototype and BA.1 strains

To address the potential risk of enhancement of the infectivity and vaccine escape of SARS-CoV-2 in animals owing to mutations within the S protein RBD region, we designed an S-trimer bivalent subunit vaccine composed of the S-trimer proteins of the original strain and the BA.1 strain carrying Y453F and N501T double-point mutations. According to the experimental procedure shown in Fig. 4a, ACE2 transgenic mice received the first and second doses of subcutaneous immunization on the nape of the neck on days 0 and 21, respectively. The PBS group was used as a control. We collected sera on days 21 and 35 after the first immunization to evaluate the humoral immunity induced by the bivalent subunit vaccine. ELISA was used to measure the levels of specific IgG antibodies in immune sera against different S proteins from the original strain, BA.1 strain, and the mutants carrying the Y453F and N501T double-point mutations, named as S-prototype, S-BA.1, and S-BA.1 (Y453F-N501T), respectively. As shown in Fig. 4b and c, the mean IgG titers of immune sera against S-prototype, S-BA.1, and S-BA.1 (453F-501T) were 2630, 2694, and 2449, respectively, on day 21 after the first immunization and further increased to 50,582, 48,968, and 44,668, respectively, on day 35 after the first immunization (i.e., day 14 after the second immunization). These results indicate that the bivalent subunit vaccine induced the production of high levels of antibodies against all three types of S proteins in mice. Furthermore, we tested the neutralizing activity of immune sera against pseudoviruses corresponding to the above three types of S proteins. The assay results showed that the geometric mean titers (GMTs) of serum neutralizing antibodies against pseudoviruses S-prototype, S-BA.1, and S-BA.1 (453F-501T) were 2641, 2945, and 2800, respectively (Fig. 4d), indicating a strong inhibition of the three types of pseudoviruses by the immune sera.

Next, to further evaluate the protective effect of the bivalent subunit vaccine, we carried out a vaccination challenge protection test in K18-hACE2 transgenic mice using two typical SARS-CoV-2 live viruses, SARS-CoV-2 prototype, and BA.1 strains, respectively (Fig. 4e). As shown in Figs. 4f–4k, the bivalent subunit vaccine protected K18-hACE2 transgenic mice against both SARS-CoV-2 prototype and BA.1 strains by alleviating weight loss, reducing viral load in the lungs, and improving lung pathological damage. Moreover, the vaccines exhibited identical protective efficacy in hamsters (Supplementary Fig. S3).

3.5. The bivalent subunit vaccine efficiently induces high-titer and Longlasting cross-neutralizing antibody production and protects cats against SARS-CoV-2 prototype strain

To evaluate the safety and efficacy of the SARS-CoV-2 bivalent subunit vaccine in cats, animal experiments were performed according to the procedures listed in Fig. 5a. Twelve British Shorthair cats were randomly and equally divided into vaccine immunization and PBS control groups. The first and second doses of subcutaneous immunization in the neck nape were administered on days 0 and 21, respectively. During the first and second immunizations, vaccine safety was evaluated. The vaccine was well tolerated and did not cause any local or systemic adverse reactions. In addition, no abnormal weight loss, abnormal food intake and elevated body temperature were observed. Blood samples were collected from all cats for antibody analysis 21 and 35 days after the first immunization. ELISA results showed that the GMT IgG titers of immune sera against S-prototype, S-BA.1, and S-BA.1 (453F-501T) were 3423, 3674, and 3780, respectively, on day 21 after the first immunization, and 40,750, 48,679, and 47,176, respectively, on day 35 after the first immunization (Fig. 5b and c). The neutralizing assay showed that immune sera collected on day 35 after the first immunization had a high degree of neutralizing activity against both pseudoviruses and live viruses. The GMTs of serum neutralizing antibodies against pseudoviruses S-prototype, S-BA.1, and S-BA.1 (453F-501T) and live viruses SARS-CoV-2 prototype and BA.1 were 4357, 5138, 4181, 1178, and 1173, respectively (Figs. 5d-5f).

We evaluated the protective effects of this bivalent subunit vaccine in vivo. Each cat was infected with the SARS-CoV-2 prototype strain at a dose of  $1 \times 10^6$  TCID50 via the intranasal route 35 days after the first immunization. As shown in Fig. 5g and h, the SARS-CoV-2 prototype strain efficiently replicated in the respiratory tracts of cats in the PBS control group. In contrast, the replicative ability of SARS-CoV-2 prototype was significantly reduced in the trachea and lung tissues of cats in the vaccinated group on days 3 and 5 after infection. Hematoxylin-eosin (HE) staining revealed that on days 3 and 5 after infection, the PBS group exhibited typical characteristics associated with COVID-19 lesions, including significant thickening of the alveolar walls, detachment of bronchial epithelial cells, and infiltration of mononuclear inflammatory cells into the alveoli. Moreover, a large amount of fibrin exudate was observed in the alveoli. In contrast, the alveolar structure of cats in the vaccine-immunized group was intact, and no obvious histopathological changes were observed. Moreover, the immunohistochemical analysis results showed that the SARS-CoV-2 N antigen was present in the fibrin exudate on the alveolar walls and alveolar cavities of the PBS group, whereas no antigen expression was observed in the vaccinated group (Fig. 5i).

Additionally, we evaluated the dynamic changes in cat serum antibodies induced by the bivalent subunit vaccine according to the experimental procedure shown in Fig. 5j. The ELISA results revealed that antibodies were detected in all cats two weeks after the first immunization; the antibody titer was highest five weeks after the first immunization and remained at a relatively high level 34 weeks after the first immunization (Fig. 5k). We also evaluated the efficacy of the bivalent subunit vaccine in dogs. Similar to its effect in cats, the vaccine safely and efficiently induced specific antibody production against SARS-CoV-2 in dogs (Supplementary Fig. S4). Taken together, our data demonstrate that the bivalent subunit vaccine induced production of high-titer and long-lasting SARS-CoV-2-specific antibodies in cats, robustly induced cross-neutralization of potential high-risk SARS-CoV-2 variants, and protected cats against infection caused by the SARS-CoV-2 prototype strain.

#### 4. Discussion

The origin of SARS-CoV-2 remains unclear; however, it has been demonstrated to have a broad host range. Currently, more than 30

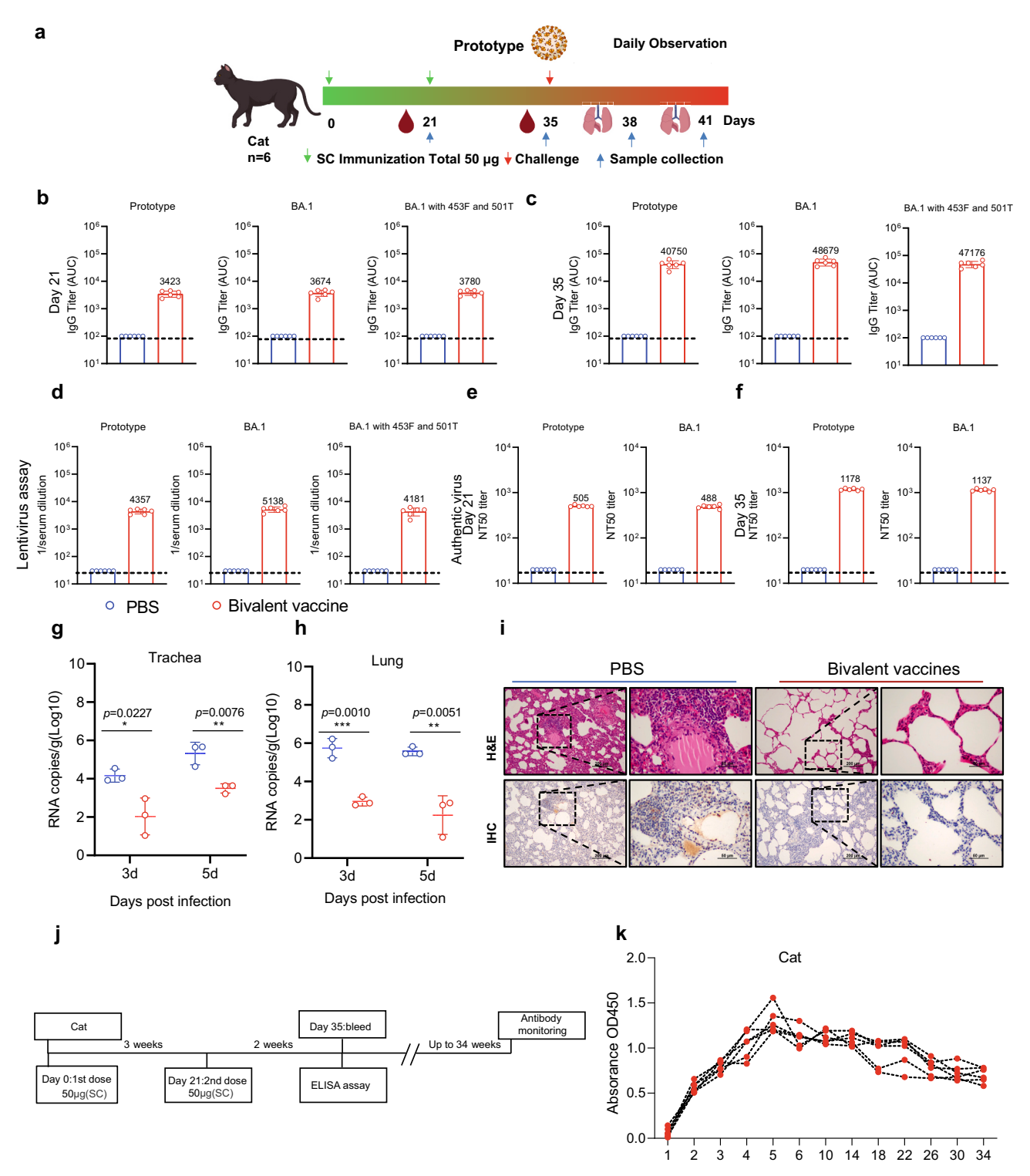


Fig. 5. The SARS-CoV-2 bivalent subunit vaccine prevents SARS-CoV-2 prototype infection in cats. (a) Schematic diagram of the immunization, blood collection, challenge, and sample collection processes in cats. (b) Serum antibody binding to SARS-CoV-2 prototype, BA.1, and Y453F-N501T double-site mutant RBD proteins as measured by ELISA on day 21. (c) Serum antibody binding to SARS-CoV-2 prototype, BA.1, and the Y453F-N501T double-site mutant RBD proteins as measured by ELISA on day 35 (n = 6 cats per group; GMTs are indicated at the top of the boxes, and LOD is shown by dotted lines). (d) Neutralizing activity of serum against pseudoviruses displaying the spike proteins of SARS-CoV-2 prototype, BA.1, and Y453F-N501T double-site mutants on day 35 (n = 6 cats per group, one experiment; GMTs are indicated at the top of the boxes, and LOD is shown by dotted lines). (e) Neutralizing activity of serum against SARS-CoV-2 prototype and BA.1 viruses on day 21 (n = 6 cats per group, one experiment; GMTs are indicated at the top of the boxes, and LOD is shown by dotted lines). (f) Neutralizing activity of serum against SARS-CoV-2 prototype and BA.1 viruses on day 35 (n = 6 cats per group, one experiment; GMTs are indicated at the top of the boxes, and LOD is shown by dotted lines). (g-h) Viral RNA levels in the trachea and lung tissues at 3 and 5 dpi. (i) Hematoxylin-eosin and indirect immunofluorescence staining of lung sections collected at 3 dpi from cats exposed to the SARS-CoV-2 prototype strain and immunized with either control PBS or the bivalent vaccine. Representative images are shown at moderate (middle; scale bars, 200  $\mu$ m) and high magnifications (bottom; scale bars, 50  $\mu$ m). (j) Schematic of the immunization, blood collection, and antibody monitoring procedures. (k) Serum antibody binding to RBD protein as measured by ELISA.

animal species are susceptible to SARS-CoV-2. [25,26] In general, the infectivity of SARS-CoV-2 in other animals is much lower than that in humans. However, with the continued spread of SARS-CoV-2, various new variants have been isolated globally, some of which could exhibit increased infectivity in animals. Once introduced into animal hosts, novel adaptive mutations may appear quickly and pose a serious risk of outbreak of SARS-CoV-2 infection in humans. [9] In fact, SARS-CoV-2 has spread among some animal populations, such as farmed minks and free-ranging white-tailed deer. [27] Therefore, assessing the impact of these mutations on the binding affinity between SARS-CoV-2 and ACE2 receptors in susceptible animals is critically important, particularly in companion animals such as cats and dogs, which are in close contact with humans. In this study, we analyzed the impact of key mutation sites within the RBD region on the affinity between RBD and ACE2. The results showed that the K417T, Y453F, Q493K, Q498H, and N501T mutations significantly enhance the binding affinity of RBD to cat ACE2. The interaction between the SARS-CoV-2 S protein and ACE2 receptor determines viral host tropism and cell entry. [28] Therefore, our data suggest that these five mutations could enhance the infectivity of SARS-CoV-2 in cats.

In addition to affecting host adaptation, antibody escape is an important threat caused by RBD mutations. [29] Mutations related to antibody escape significantly decrease the efficacy of vaccines and therapeutic antibodies, thereby resulting in tremendous hazards. For example, E484K can reduce the neutralization titers of immune sera or convalescent plasma by more than an order of magnitude. [30] Variants containing E484K, such as lineages B.1.35 and P.1, pose a serious threat to human health. [31] Here, we demonstrated that the Y453F and N501T mutations significantly reduced the neutralizing activity of the immune serum whose production was induced by the SARS-CoV-2 prototype strain-inactivated vaccine in cats, whereas the K417T, Q493K, and Q498H mutations had no significant impact. These results suggest that the Y453F and N501T mutations pose a higher risk than those associated with the other three mutations.

Animal-derived variants have raised concerns regarding the threat of occurrence of severe pandemics. However, risk assessments of the relevant key mutations are scarce. Previous studies have indicated that both the Y453F and N501T mutations are closely related to animalderived SARS-CoV-2 variants [22]. They are present in the SARS-CoV-2 strains detected in farmed minks, white-tailed deer, and companion animals such as dogs and cats at relatively high frequencies. [27] In this study, we demonstrated that Y453F and N501T mutations not only significantly reduced the neutralizing ability of immune sera, but also synergistically enhanced the binding of RBD to cat ACE2. These risks of Y453F and N501T mutations are not confined to cats because these mutations pose a similar threat in dogs and minks [20,22]. Moreover, the SARS-CoV-2 RBD Y453F and N501T mutations may potentially lead to a high risk of cross-species transmission among multiple animal species. These findings suggest that the Y453F and N501T mutations pose a significant public health threat. Therefore, although these two mutations are not present in any VOCs, they should be seriously considered. Currently, vaccines are the most cost-effective tools for preventing and controlling SARS-CoV-2 infections. [32] However, the continuous emergence of various SARS-CoV-2 variants and the rapid waning of vaccine-elicited immunity have seriously threatened the effectiveness of existing vaccines. [33] Therefore, considering the threat of animal-related high-risk variants, development of a new vaccine against SARS-CoV-2 that can provide lasting and effective crossprotection is necessary. Here, we designed a bivalent subunit vaccine by introducing the Y453F and N501T mutations based on the BA.1 strain sequence, which can robustly induce broad-spectrum antibody responses. In vivo, the bivalent subunit vaccine effectively protected human ACE2-expressing transgenic mice against infections caused by the prototype and BA.1 strains and cats against infections caused by the prototype strain. In vitro, the immune serum induced by the bivalent subunit vaccine efficiently cross-neutralized pseudoviruses S-prototype,

S-BA.1, and S-BA.1 (453F-501T) and live viruses SARS-CoV-2 Prototype and BA.1. Currently, with the continuous evolution of the SARS-CoV-2 virus, new variants such as JN.1, KP.1, and KP.3 are constantly emerging. However, the potential for cross-species transmission of these variants in felid species remains to be elucidated. Certainly, this vaccine may also face the same issue of breakthrough infections as existing commercial vaccines, which requires further verification.

Notably, the antibody monitoring results revealed that vaccine-elicited immunity remained at a high level seven months after the first immunization. This sustained immune response may be attributed, at least in part, to the synergistic adjuvant effects of CpG oligonucleotides and GEL02, where CpG-1018 serves as a potent TLR9-targeting vaccine adjuvant with marked species specificity (76 % homology between human and murine TLR9). While the conventionally defined murine-specific AACGTT motif (CpG-1018) demonstrated good adjuvant activity in hepatitis B vaccine trials, more importantly, sequences containing the TCGT core motif exhibit cross-species immunostimulatory effects [34,35]. This study reveals that CpG-1018 effectively enhances vaccine-induced immune responses in felines, though its feline TLR9 recognition mechanism requires further elucidation.

#### 5. Conclusions

In summary, we assessed the potential risk of SARS-CoV-2 infection associated with key mutations within the RBD of SARS-CoV-2 in cats. Our data revealed that Y453F and N501T mutations significantly enhance the affinity between the RBD and cat ACE2 and reduce the neutralizing activity of immune serum induced by the SARS-CoV-2 prototype strain-inactivated vaccine in cats. The Y453F and N501T mutations are also associated with a risk of infection in other animals, such as dogs and minks. Therefore, to address the potential threats of Y453F and N501T mutations, we developed a bivalent subunit vaccine that exhibits excellent cross-protective efficacy against the original strains SARS-CoV-2 prototype and Omicron BA.1, and a variant of BA.1 containing 453F and 501 T mutations. The vaccine will facilitate blockage of the potential covert transmission of the novel variants between humans and animals.

#### CRediT authorship contribution statement

Ya Zhao: Writing – original draft, Software, Project administration, Conceptualization. Zongzheng Zhao: Visualization, Supervision, Resources, Data curation. Chuxing Cheng: Software. Mingyao Tian: Supervision, Formal analysis, Conceptualization. Qiang Zhang: Writing – review & editing, Funding acquisition, Formal analysis, Data curation, Conceptualization. Meilin Jin: Writing – review & editing, Visualization, Conceptualization.

#### Declaration of competing interest

The authors declare that they have no known competing financial interests or personal relationships that could have appeared to influence the work reported in this paper.

#### Acknowledgements

This work was supported by the Hubei Science and Technology Major Project (2021ACB004) and the Program of Hubei Jiangxia Laboratory (grant no. JXBS003). We are deeply grateful to all staff from the Wuhan National Biosafety Laboratory, Chinese Academy of Sciences, Wuhan, as well as those from the Changchun Veterinary Research Institute Biosafety Laboratory, Chinese Academy of Agricultural Sciences, Changchun.

#### Appendix A. Supplementary data

Supplementary data to this article can be found online at https://doi.org/10.1016/j.vaccine.2025.127685.

#### Data availability

Data will be made available on request.

#### References

- [1] Romanello M, McGushin A, Di Napoli C, Drummond P, Hughes N, Jamart L, et al. The 2021 report of the lancet countdown on health and climate change: code red for a healthy future. Lancet 2021;398:1619–62.
- [2] Liu YH, Hu GW, Wang YY, Ren WL, Zhao XM, Ji FS, et al. Functional and genetic analysis of viral receptor ACE2 orthologs reveals a broad potential host range of SARS-CoV-2. P Natl Acad Sci USA 2021:118.
- [3] Gao GRF, Wang L. COVID-19 expands its territories from humans to animals. China Cdc Weekly 2021;3:855–8.
- [4] Zhou P, Shi ZL. SARS-CoV-2 spillover events. Science 2021;371:120-2.
- [5] Zhang Q, Zhang H, Gao J, Huang K, Yang Y, Hui X, et al. A serological survey of SARS-CoV-2 in cat in Wuhan. Emerg Microbes Infect 2020;9:2013–9.
- [6] Zhao Y, Yang Y, Gao J, Huang K, Hu C, Hui X, et al. A serological survey of severe acute respiratory syndrome coronavirus 2 in dogs in Wuhan. Transbound Emerg Dis 2022;69:591–7.
- [7] Tan CCS, Lam SD, Richard D, Owen CJ, Berchtold D, Orengo C, et al. Transmission of SARS-CoV-2 from humans to animals and potential host adaptation. Nat Commun 2022:13.
- [8] Sparrer MN, Hodges NF, Sherman T, VandeWoude S, Bosco-Lauth AM, Mayo CE. Role of spillover and spillback in SARS-CoV-2 transmission and the importance of one health in understanding the dynamics of the COVID-19 pandemic. J Clin Microbiol 2023;61.
- [9] Munnink BBO, Sikkema RS, Nieuwenhuijse DF, Molenaar RJ, Munger E, Molenkamp R, et al. Transmission of SARS-CoV-2 on mink farms between humans and mink and back to humans. Science 2021;371:172–7.
- [10] Piplani S, Singh PK, Winkler DA, Petrovsky N. In silico comparison of SARS-CoV-2 spike protein-ACE2 binding affinities across species and implications for virus origin (vol 11, 13063, 2021). Sci Rep-Uk 2021;11.
- [11] Lan J, Ge J, Yu J, Shan S, Zhou H, Fan S, et al. Structure of the SARS-CoV-2 spike receptor-binding domain bound to the ACE2 receptor. Nature 2020;581:215–20.
- [12] Walls AC, Park YJ, Tortorici MA, Wall A, McGuire AT, Veesler D. Structure, function, and antigenicity of the SARS-CoV-2 spike glycoprotein. Cell 2020;183: 1735
- [13] Jackson CB, Farzan M, Chen B, Choe H. Mechanisms of SARS-CoV-2 entry into cells. Nat Rev Mol Cell Biol 2022;23:3–20.
- [14] Yang J, Wang W, Chen Z, Lu S, Yang F, Bi Z, et al. A vaccine targeting the RBD of the S protein of SARS-CoV-2 induces protective immunity. Nature 2020;586:572–7.
- [15] Richmond P, Hatchuel L, Dong M, Ma B, Hu B, Smolenov I, et al. Safety and immunogenicity of S-trimer (SCB-2019), a protein subunit vaccine candidate for COVID-19 in healthy adults: a phase 1, randomised, double-blind, placebocontrolled trial. Lancet 2021;397:682–94.

- [16] Baden LR, El Sahly HM, Essink B, Kotloff K, Frey S, Novak R, et al. Efficacy and safety of the mRNA-1273 SARS-CoV-2 vaccine. N Engl J Med 2021;384:403–16.
- [17] Chi XY, Yan RH, Zhang J, Zhang GY, Zhang YY, Hao M, et al. A neutralizing human antibody binds to the N-terminal domain of the spike protein of SARS-CoV-2. Science 2020;369:650.
- [18] Tang XL, Wu CC, Li X, Song YH, Yao XM, Wu XK, et al. On the origin and continuing evolution of SARS-CoV-2. Natl Sci Rev 2020;7:1012–23.
- [19] Ai J, Wang X, He X, Zhao X, Zhang Y, Jiang Y, et al. Antibody evasion of SARS-CoV-2 omicron BA.1, BA.1.1, BA.2, and BA.3 sub-lineages. Cell Host Microbe 2022;30 (1077–83):e4.
- [20] Ren WL, Lan J, Ju XH, Gong ML, Long QX, Zhu ZH, et al. Mutation Y453F in the spike protein of SARS-CoV-2 enhances interaction with the mink ACE2 receptor for host adaption. PLoS Pathog 2021:17.
- [21] Alenquer M, Ferreira F, Lousa D, Valério M, Medina-Lopes M, Bergman ML, et al. Signatures in SARS-CoV-2 spike protein conferring escape to neutralizing antibodies. PLoS Pathog 2021:17.
- [22] Su C, He JH, Han PC, Bai B, Li DD, Cao J, et al. Molecular basis of mink ACE2 binding to SARS-CoV-2 and its mink-derived variants. J Virol 2022;96.
- [23] Huang K, Zhang Y, Hui X, Zhao Y, Gong W, Wang T, et al. Q493K and Q498H substitutions in spike promote adaptation of SARS-CoV-2 in mice. EBioMedicine 2021;67:103381.
- [24] Imai M, Iwatsuki-Horimoto K, Hatta M, Loeber S, Halfmann PJ, Nakajima N, et al. Syrian hamsters as a small animal model for SARS-CoV-2 infection and countermeasure development. P Natl Acad Sci USA 2020;117:16587–95.
- [25] Shi J, Wen Z, Zhong G, Yang H, Wang C, Huang B, et al. Susceptibility of ferrets, cats, dogs, and other domesticated animals to SARS–coronavirus 2. Science 2020; 368:1016–20.
- [26] Halfmann PJ, Hatta M, Chiba S, Maemura T, Fan S, Takeda M, et al. Transmission of SARS-CoV-2 in domestic cats. N Engl J Med 2020;383:592–4.
- [27] Zhao J, Kang M, Wu HY, Sun BW, Baele G, He WT, et al. Risk assessment of SARS-CoV-2 replicating and evolving in animals. Trends Microbiol 2024;32:79–92.
- [28] Wang QH, Zhang YF, Wu LL, Niu S, Song CL, Zhang ZY, et al. Structural and functional basis of SARS-CoV-2 entry by using human ACE2. Cell 2020;181:894.
- [29] Li CJ, Chang SC. SARS-CoV-2 spike S2-specific neutralizing antibodies. Emerg Microbes Infec 2023:12.
- [30] Harvey WT, Carabelli AM, Jackson B, Gupta RK, Thomson EC, Harrison EM, et al. SARS-CoV-2 variants, spike mutations and immune escape. Nat Rev Microbiol 2021;19:409–24.
- [31] Wise J. Covid-19: the E484K mutation and the risks it poses. Bmj-Brit Med J 2021: 372.
- [32] Fiolet T, Kherabi Y, MacDonald CJ, Ghosn J, Peiffer-Smadja N. Comparing COVID-19 vaccines for their characteristics, efficacy and effectiveness against SARS-CoV-2 and variants of concern: a narrative review. Clin Microbiol Infect 2022;28:202–21.
- [33] Subbarao K. The success of SARS-CoV-2 vaccines and challenges ahead. Cell Host Microbe 2021;29:1111–23.
- [34] Rankin R, Pontarollo R, Ioannou X, Krieg AM, Hecker R, Babiuk LA, et al. CpG motif identification for veterinary and laboratory species demonstrates that sequence recognition is highly conserved. Antisense Nucleic Acid Drug Dev 2001; 11:333-40.
- [35] Hyer RN, Janssen RS. Immunogenicity and safety of a 2-dose hepatitis B vaccine, HBsAg/CpG 1018, in persons with diabetes mellitus aged 60-70 years. Vaccine 2019;37:5854–61.